Journal of Hydrology 472–473 (2012) 340–354

Contents lists available at SciVerse ScienceDirect

Journal of Hydrology

journal homepage: www.elsevier.com/locate/jhydrol

Numerical modeling of hydrodynamics and sediment transport in lower Mississippi at a proposed delta building diversion

Ehab A. Meselhe [a,*], Ioannis Georgiou [b], Mead A. Allison [c], John A. McCorquodale [d]

[a] The Water Institute of the Gulf, Baton Rouge, LA 70825, USA
[b] Department of Earth and Environmental Sciences, University of New Orleans, New Orleans, LA 70148, USA
[c] University of Texas Institute for Geophysics, University of Texas, 10100 Burnet Road (R2200), Austin, TX 78758-4445, USA
[d] Department of Civil and Environmental Engineering, University of New Orleans, New Orleans, LA 70148, USA

ARTICLE INFO

Article history:
Received 26 January 2012
Received in revised form 14 September 2012
Accepted 20 September 2012
Available online 5 October 2012
This manuscript was handled by Corrado Corradini, Editor-in-Chief, with the assistance of Attilio Castellarin, Associate Editor

Keywords:
Mississippi River
Sediment
Diversions
Bends
Three dimensional
Lagrangian

SUMMARY

The Mississippi River Delta of south Louisiana USA is a highly engineered system with extensive levees, flood control, and diversion structures. This region is experiencing a high rate of coastal wetland loss. Solutions to divert or re-direct a portion of the River's sediment to benefit wetlands and reduce coastal land-loss are considered. The question that must be answered, regarding the impact and feasibility of sediment diversions is: What is the sediment–water ratio at a diversion? To help answer this question a numerical model of hydrodynamics and sediment transport supported by extensive field data is used to analyze a proposed sediment diversion near Myrtle Grove, Louisiana. This location is at a River Kilometer 90 above the Head of Passes – exit of the Mississippi River to the Gulf of Mexico. The numerical model showed that the location of the diversion, the size and the alignment of the diversion channel are critical parameters affecting the sediment–water ratio captured by the diversion. The analysis shows that locating the intake near a lateral sandbar increases the sediment–water ratio in the diversion. Further, the analysis shows that a larger diversion channel with a favorable alignment orientation to the flow direction in the river results in higher sediment–water ratio.

1. Introduction

The Mississippi River Delta is approximately 25,000 km^2, and consists of wetlands, bayous, shallow bays and emergent ridges formed during the late Holocene (~6000 yBP to present) progradation of delta plain distributaries of the Mississippi River (Coleman et al., 1998). In the 1960s it was first recognized that the Mississippi delta region of south Louisiana was experiencing coastal wetland land loss rates that are among the highest on Earth (Gagliano et al., 1981; Day et al., 2000). Rates reached a maximum of 102 km^2/y in the 1970s (Barras et al., 2003), and although rates have decreased somewhat since then (61 km^2 from 1990 to 2000; Barras et al., 2003), Hurricanes Katrina and Rita in 2005 showed that individual cyclonic storms could account for a significant episodic wetland loss (the two storms caused a combined 526 km^2 of land loss in South Louisiana; Barras, 2009). Two main mechanisms have been suggested for rebuilding marsh areas: water and sediment diversions from the Mississippi and its Atchafalaya distributary, and long-distance pipelines to spoil dredged materials from the river beds as well as inland and offshore deposits. The focus of the present study is to develop numerical modeling tools to investigate Mississippi River diversions in support of testing restoration alternatives critical to the future of the Mississippi Delta region.

Large River diversions are defined here as >1420 cms (50,000 cfs). With the exception of West Bay Diversion at river kilometer (RK) 15.4 above Head of Passes (HOP), none of the existing water diversions on the river between Baton Rouge and the Gulf of Mexico are dedicated as sediment diversions: the remainder are freshwater diversions for controlling salinity intrusion or are designed for flood control. However, the US Army Corps of Engineers has conducted a series of examinations of large structure design and operation as part of project-specific and holistic coastal restoration studies (ABFS, 1982; USACE, 1984; MRSNFR, 2000; LCA, 2004; LACPR, 2009). Also, the Bonnet Carré Spillway is an existing gated water exit with a capacity of 7080 cms (250,000 cfs) for protection of New Orleans and areas lower on the river from extreme river floods. It differs from water and sediment diversions that are the focus of this discussion in that it is not used annually (only opened during years when flows exceed 35,396 cms [1.25 million cfs]), cannot be operated below a certain river stage, and is not

* Corresponding author. Tel.: +1 225 456 1556.
E-mail address: emeselhe@thewaterinstitute.org (E.A. Meselhe).

0022-1694/$ - see front matter © 2012 Elsevier B.V. All rights reserved.
http://dx.doi.org/10.1016/j.jhydrol.2012.09.043

managed to optimize either water and sediment delivery for beneficial coastal restoration or preservation.

As indicated above, since the installation of the Mississippi River flood protection (levees) and navigation works, Louisiana's coastal wetlands have been deprived of most of their historic sediment load that the river is now transporting to the Gulf of Mexico (Allison and Meselhe, 2010; Meselhe et al., 2005). Therefore, alternative solutions to recover or re-direct a portion of this valuable sediment to benefit Louisiana's coast are currently being considered. For such efforts to be successful, the impact of restoration projects on the river and on the surrounding wetlands and water bodies must be considered. The numerical modeling of hydrodynamics, sediment transport and other characteristics of the Mississippi River will help to assess the potential impacts of the various options for the restoration of the Louisiana coast (Meselhe et al., 2005; Kheiashy et al., 2010; Rego et al, 2010; Pereira et al, 2009).

The focus of this study is to setup an appropriate computer flow model to analyze and optimize the design of a sediment diversion. The FLOW3D model was selected to perform this analysis. There are many research and commercial codes available with varying degrees of strengths and limitations. The FLOW3D model was selected here due to its capability of modeling detailed hydraulic structures, complex geometries, and the ability to model suspended sediment with multiple size classes. It uses a Lagrangian approach to track the various sediment size classes. The feature is critical here to allow for examining the ability of a diversion structure to capture and divert sediment from the main river into the outfall channel. The Myrtle Grove diversion site was chooses as a test bed for the analysis (Figs. 1 and 2). The proposed diversion is on the right descending bank of the Mississippi River (west bank). The intent of the diversion is to provide sediment to the Barataria Basin. The objective is to build land in the receiving basin near-term through the use of dedicated dredged material from the Mississippi channel bed. This land building capacity will be sustained in the long-run in this subsiding basin by diverting suspended sediment from the Mississippi River. The diversion is to be operated only during the high flow season (December–June) of the Mississippi River when suspended sediment loads, and particularly sand loads (>63 μm) are at a maximum. As such, the diversion will be operated in pulses that mimic the overtopping of natural levees—a strategy that has previously been implemented at the smaller Caernarvon diversion (Lane et al., 2006). This will maximize the sediment–water ratio in the diverted flow and minimize the shoaling and siltation problems in the Mississippi River channel.

2. Field data

Field data were collected to calibrate and validate the numerical model. The field observations are fully described in Allison (2011), but are summarized here. Seven main field surveys were carried out to capture a range of Mississippi River water discharges at Myrtle Grove and a comparative site at Magnolia (RK75)—October 2008, April 2009, May 2009, April 2010, May 2010, March 2011 and May 2011. The boat surveys were carried out on a 7 m vessel (R/V *Lake Itasca*) at discharges ranging from 11,900 cms (October 2008) to 34,800 cms (May 2011). Bathymetry of the entire Myrtle Grove model reach was conducted in the October 2008–May 2009 field studies using a Reson 8101 Seabat multibeam bathymetric profiler. Water velocities and discharges were measured at selected river cross-sections (and longitudinal profiles) using RD Instruments 600 and 1200 kHz Workhorse acoustic Doppler current profilers (ADCPs). Cross-sectional water discharges were converted to suspended sediment fluxes using three or more vertical sampling stations along the profile, sampled at five water depths (e.g., 0.1, 0.3, 0.5, 0.7, and 0.9 total water depth at each station) using a 91 kg, point-integrative water sampler (1 L sample volume). Vertical stations were also sampled for bed grain size using a Shipek grab sampler on several field studies. All water and bed samples were measured for percentage of sand (>63 μm) and mud using sieving and pipette analysis, and selected samples were analyzed for detailed sand grain size classes utilizing an automated settling column.

The model domain extends from RK90.1 (AHOP) to RK100.9 AHOP (Fig. 2). This river reach encompasses the potential locations for the sediment diversion site. The multi-beam data, collected by a boat, often does not provide coverage in shallow areas (less than 3–5 m water depth) near the bank lines. Hence, this portion of the bathymetry was supplemented by the US Army Corps of Engineers decadal single beam surveys in order to have fully cross-sectional bathymetric information of this river reach. Over bank topographic data were used to supplemented the bathymetry using airborne LiDAR data (http://atlas.lsu.edu).

3. Numerical modeling

A three-dimensional model is used to develop an understanding of the complex flow field at a river bend and examine the interaction between flow and sediment. It is important to identify a model capable of resolving the details of the spatial distribution of suspended sediment near the lateral bar on the right descending bank (upstream of the Myrtle Grove bend), through the river bend and across toward the point bar on the left descending bank (downstream of the Myrtle Grove bend). Overall, the objectives of the modeling effort include capturing the complex three-dimensional flow field in the vicinity of possible diversion sites, quantifying the sand load available for diversion under various flow conditions, quantifying the fraction of the available sand load that can be diverted for various conveyance channel alignments and configurations, and investigating the potential for shoaling and headcutting as a result of sediment diversions. The FLOW-3D model by Flow Science® was selected to perform the analysis as it is capable of resolving the dominant physical processes with acceptable computational efficiency.

3.1. Hydrodynamics

FLOW-3D is a three dimensional model where fluid motion is described with non-linear transient, second-order differential Navier Stokes equations. The numerical algorithm used in FLOW-3D is based on both finite difference and finite volume methods applied to a structured computational grid. Structured grids are known for their computational efficiency and ease of discretizing the flow domain. The finite volume method used in FLOW-3D derives directly from the integral form of the conservation laws for fluid motion, and therefore, retains the conservation properties. The model is capable of capturing complex geometries. This is an essential feature due to the typical irregular river bottom bathymetry including ripples and sand bars, and irregular bank boundaries as well as the need to include the geometry of the diversion structure. The method used in FLOW-3D (called FAVOR™, Hirt and Sicilian, 1985) is an efficient approach that resolves complex geometries while maintaining the use of structured computational grids (Fig. 3). The cell volume occupied by the fluid is captured, and the ratio of the volume occupied by fluid to the total cell volume is calculated. This ratio is referred to as the Volume of Fluid (VOF) and it is incorporated into the mass conservation equations. As such, the geometry of obstacles (river bottom, bank lines, or hydraulic structures) is described through the area fraction at all cell faces and the fluid volume fraction within the cell. In essence, FLOW-3D takes advantage of the computational speed and

Fig. 1. Map of the lowermost Mississippi River showing the potential diversion site at Myrtle Grove (the diversion site is immediately downstream of Station 2).

efficiency of structured grids while being fully capable of resolving complex geometries.

FLOW-3D is also capable of capturing the water free-surface accurately. Previously, FLOW-3D used the two-fluid Volume of Fluid (VOF) method to capture free-surface variations (Hirt and Nichols, 1981). However, this method may result in diffusion of the interface and is computationally expensive. Other approaches such as Meselhe and Sotiropoulos (2000) also confirm the computational challenges to capture the water surface variations. The new approach adopted in FLOW-3D is called TrueVOF® (Barkhudarov, 2004). This approach computes the advection of fluid to all neighboring cells according to the orientation of the fluid within the cell under consideration. It does not compute the dynamics in the void region (Fig. 4). Rather, it applies pressure and velocity boundary conditions to compute the sharp free surface interface.

The governing equations used in FLOW-3D can be found in (Flow Science, 2010, FLOW-3D user Manual). One of the critical factors that determine the ability of a numerical model to capture complex flow patterns is the turbulence closure model used as part of the flow governing equations. FLOW-3D includes several turbulence closure models, namely Prandtl mixing length, One-equation transport, two-equation k–ε transport, Renormalized group theory (RNG), and Large Eddy Simulation (LES) models. The two-equation turbulent closure models are widely used due to their relative computational efficiency and adequate performance for wide-range of practical applications (e.g. Meselhe et al., 2000; Muste et al., 2001).

For the simulations performed here, the Renormalization-Group (RNG) method (Yakhot and Orszag, 1986; Yakhot and Smith, 1992) was used. The RNG model applies statistical methods to the derivation of turbulent kinetic energy and its dissipation rate. The main difference between the RNG method and the k–ε model is that the constants (appearing in the governing equations of the turbulence model) are found empirically in the standard k–ε model whereas they are derived explicitly in the

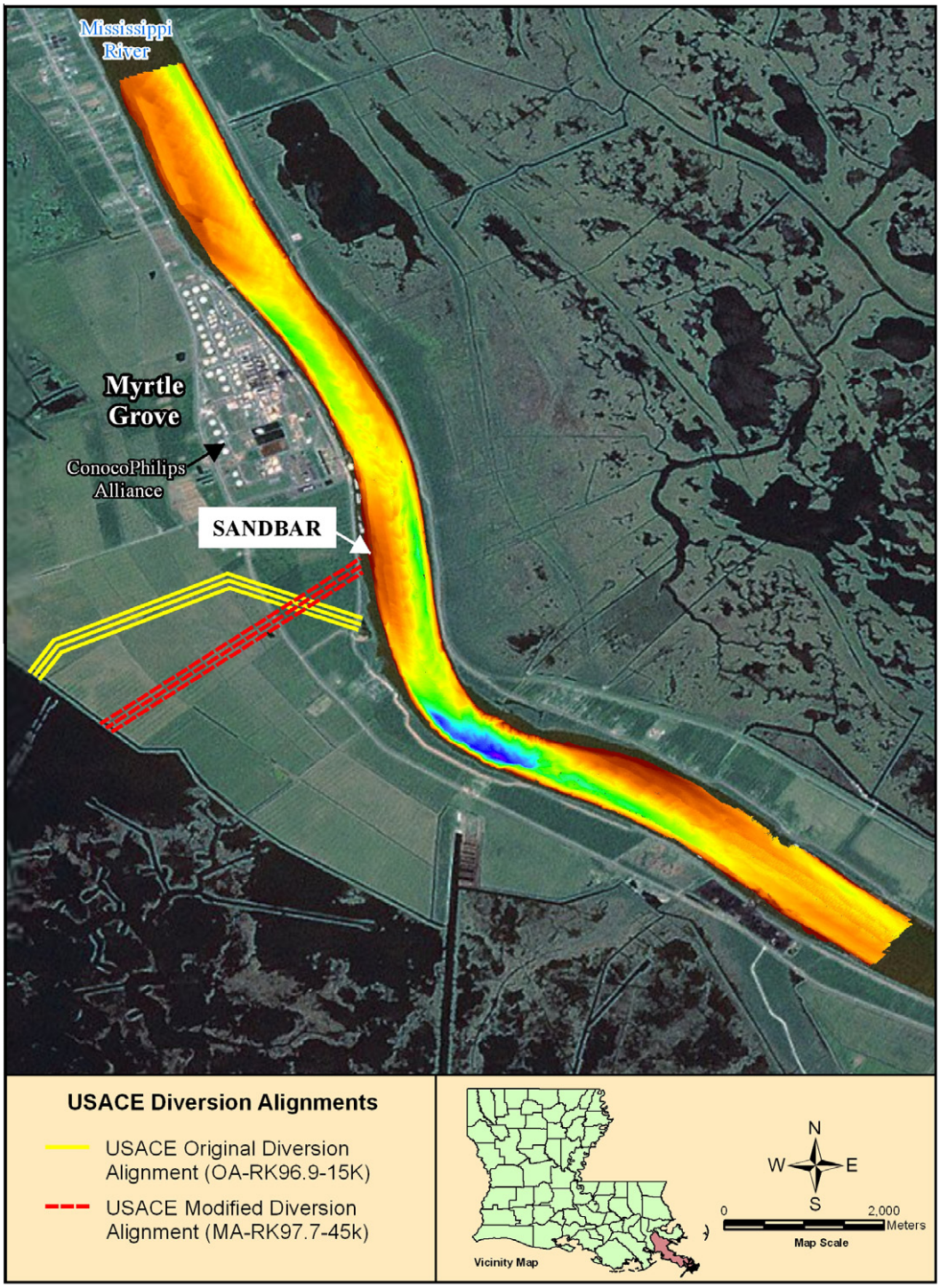

Fig. 2. Layout of the original and modified diversion alignments at Myrtle Grove.

RNG model. The RNG approach appears to have wider applicability than the standard k–ε model. The RNG model was selected because is more adequate for riverine applications with flows having strong shear regions.

3.2. Sediment transport

The traditional modeling approach for modeling suspended sediment is to treat it as a state-variable using the advection–diffusion equation while including a fall-velocity term. In this study, the focus is capturing suspended sand into the sediment diversion. Harnessing sediment moving along the bed is not possible due the depth of the Lower Mississippi River. As such, the research focused on suspended sediment. A Lagrangian approach has been identified to simulate the transport of suspended sediment. A cluster of discrete mass particles were released at the upstream end of the model domain. These particles were assigned variable sizes and mass (ranging from silt; 32 μm, to sand; 250 μm). This approach is well suited to estimating the spatial distribution of each sediment size class in the river section under study, by tracking the amount of each sediment size class that is diverted through a certain structure configuration.

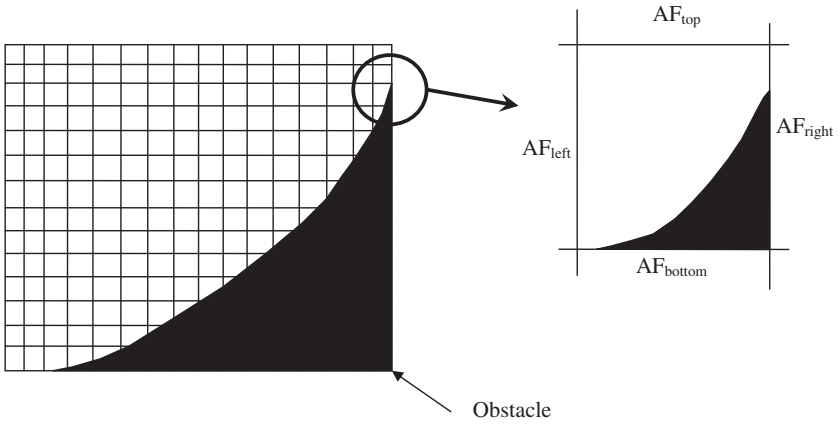

Fig. 3. Method used in FLOW-3D (FAVOR™) to capture complex geometries. (AF: is the Area of each Face of a grid cell.)

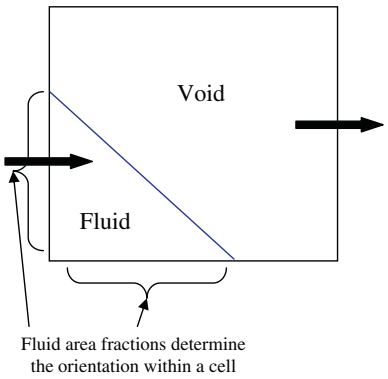

Fig. 4. Volume of Fluid (TrueVOF®) approach in FLOW-3D to capture the free-surface.

This approach is fully described in Hirt (1999). Brief description of the approach is provided here. The approach allows for multiple mass particle species to be modeled simultaneously. The fundamental equation used to model mass particles is shown below:

$$\frac{du_p}{dt} = -\frac{1}{\rho_p}\nabla P + g + \alpha(u - u') + \beta(u - u')|u - u'| \cdot \frac{\rho}{\rho_p} \quad (6)$$

where $u' = u_p + u_{diff}$, u_p and ρ_p are the particle mean velocity and density, respectively, g is gravity a other body forces, u and P are the surrounding fluid velocity and pressure whereas α and β are the drag coefficients divided by the particle's mass. The particle diffusion velocity, u_{diff}, is estimated according to a Monte Carlo technique described below. The drag coefficients, α and β are calibration coefficients. It is also possible to employ a variable drag coefficient (function of Reynolds number of the surrounding fluid).

The particle diffusion process in FLOW-3D adds an increment in position to each particle prior to establishing the new position of that given particle. Each particle is initially considered as a sediment point source. As time passes that source diffuses in all directions forming a sediment cloud with a Gaussian distribution. However, in the numerical simulation, each sediment particle remains a discrete entity. Thus the Gaussian cloud is mapped into a probability function used to transport the particle. The new position of the particle is calculated using a random number generator. Overall, a Monte Carlo approach is used to compute random shifts in the position of a given particle in each of the three coordinate directions.

There are two primary interaction mechanisms between suspended sediment and the surrounding fluid, namely, the momentum exchange and the volume displacement. The latter can typically be ignored since it is reasonable to assume that the volume concentration/displacement is small. For application where the relative difference between the particle density and fluid density is not large (such as the case with sediment and water) it is important to calculate the drag resistance to the particles as they move through the fluid. However, the total loss of momentum by this mechanism is small enough and does not have to be transferred back to the fluid. As such, it is possible (and desirable for computational speed) to compute the fluid motion then use the flow field to move particles. It should be noted that this assumption is for the suspended load and may not apply in the bed layer where the concentration of particles can be very high.

4. Model setup

A grid dependence analysis was performed and a grid of 15 m × 15 m × 2.5 m was found to be appropriate to capture the details of the complex flow pattern observed in the field data. The grid cell sizes assessed were 100, 50, 30, 20, 15, and 10 m. These studies indicated that the solution stabilizes at cell sizes 20 m or smaller. The variations were mostly in the transverse (bank to bank) velocity distribution. As such, a grid size of 15 m was used for this study.

4.1. Boundary conditions

Discharge measured by boat-based methods was used as the upstream boundary condition, while the tail water elevation was used as the downstream boundary condition. The water flow during this field campaign used for model calibration was 19,822 cms (700,000 cfs). There is no tail water information available at the downstream end of the model domain. Therefore, numerical simulations using HEC-RAS (Davis, 2010) was used to estimate the tail water elevation, also confirmed by measurements at the Conoco-Philips station (RK101.7). The tail-water estimate was 1.9 m-NAVD88.

The model was validated with field observations in April 2010 events. The water flow during the April 2010 event was 23,786 cms (840,000 cfs). Again HEC-RAS simulations combined with information from the continuous station at Conoco-Philips (RK101.7) were used to estimate the tail water. For April 2010, tail water in the range of 1.8–2.0 m-NAVD88 was used.

5. Model calibration and validation

Flows in rivers encounter resistance or drag proportional to the roughness of the banks and bed. For the RNG turbulence transport models used herein, the roughness of the boundary is incorporated through boundary conditions for the turbulence quantities, namely the kinetic energy and its rate of dissipation. The wall-function approach is a common method to set these boundary conditions. A wall roughness coefficient in FLOW-3D is used as a calibration parameter (Flow Science, 2010). Through numerical experimentations done herein, a range of 0.04–0.08 for the roughness coefficient proved reasonable for sand-bottom river applications. For a water flow of 19,822 cms, a value of 0.06 provided a water surface slope of 0.000016 (total head drop of 0.17 m across the length of the river reach modeled here). This compares well with a water surface slope of 0.000014 (total head drop of 0.15 m) estimated by a one-dimensional model applied to the same river reach (Davis, 2010).

Field velocity profiles obtained from analysis of boat-based ADCP (shown in Fig. 5) were compared to model derived velocity profiles at selected locations. These locations were selected to match locations where sediment transport measurements were conducted using isokinetic methods. During the calibration of the model, minor adjustments to the friction factor were made until a desirable water surface slope was achieved compared to previously calibrated one dimensional model and observations. During the velocity and sediment calibration, minor adjustments to the diffusion coefficient were made (for sediment); however, during model validation no additional adjustments of any parameters in the model were applied. For consistency with the field data report by Allison (2011), the sites used in the calibration and shown in Fig. 5 are referred to as *MGup*, *MGbend*, and *MGdown* in subsequent plots. The locations of the ADCP transects are shown with solid white lines while open circles indicate the locations of the isokinetic casts.

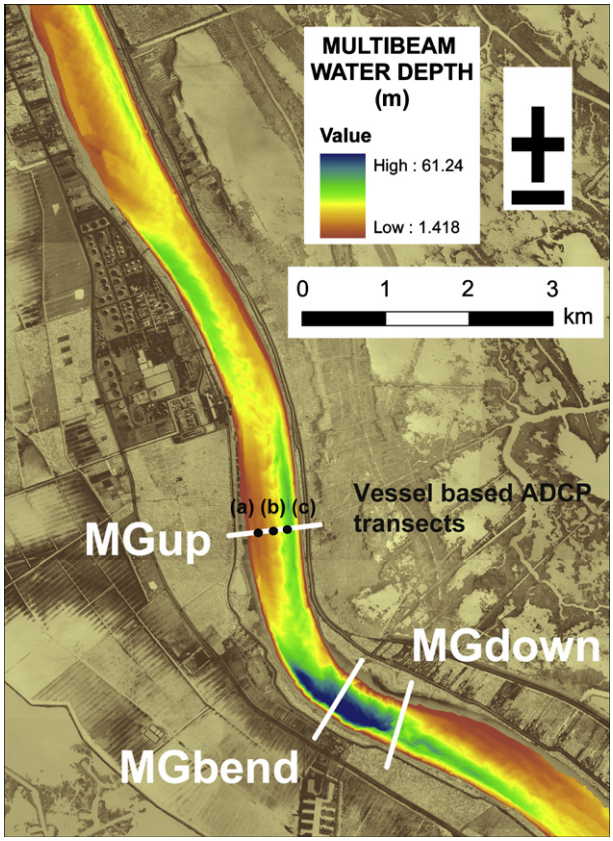

Fig. 5. Locations were vessel based ADCP and suspended sediment load casts were used in the model calibration and validation.

5.1. Preparation of hydro-acoustic data

Velocities extracted from the boat-based ADCP surveys were spatially reduced using averaging methods. Data reduction was performed in both the horizontal direction (along a river transect) and in the vertical direction (from the water surface down to the river bed). The horizontal averaging was conducted on 10, 20, and 30 m intervals, while the vertical averaging was performed every 1 m. Since the instrument collects data at 1 Hz, several horizontal ensembles are included in the horizontal averaging, while the 0.5 m bin interval in the vertical allow for averaging of only two data points. The reduced data showed velocity trends more effectively and provided more clear comparison with model simulations. A schematic of the location and general methodology is shown in Fig. 6.

At each boat-based ADCP transect a number of ensembles (or number of observations) along that transect, n, was defined. Using a 10 m (space) window, an averaging process of the ensembles across the river in the direction of the vessel was performed (transverse direction using heading from the DGPS signal). Vertical averaging was also performed over the water depth every one meter (2 bins), such that:

$$\overline{U_{j,k}}, \overline{V_{j,k}}, \overline{W_{j,k}} = \frac{1}{M}\frac{1}{N}\sum_{j=1}^{M}\sum_{k=1}^{N}(U, V, M) \tag{7}$$

for $N > 0$, and $N = L$, $M > 1$, and $M = 40$, or D, where U, V, W are the east, north, and vertical velocities respectively; N (~10 m) is the number of data points in the ensemble mean of the horizontal 10-m average segment, and M (=2) is the number of vertical bins that are considered for mean from the raw ADCP data. The averaging is carried out for the entire river width (L), and for the entire river depth (D) for each ensemble segment (M, N).

5.2. General circulation patterns

Once the water surface slope was calibrated, the model's ability to produce known and observed circulation patterns within the domain and study area was evaluated. These features are re-circulation eddies (near the inside of the meander bend) and secondary circulation which is typically along the meander (described further below). Fig. 7 shows the re-circulation eddy near the left descending bank just downstream of the meander. The insert shows the map where the re-circulation zone takes place, and panel (a) shows the flow direction, (b) shows the location and (c) shows the size of this recirculation region as recorded in the field.

The other circulation feature used to test the model performance was secondary circulation. Secondary circulation is common near river meanders; capturing this was necessary in assessing the performance of the model. The model appears to capture the general secondary circulation fairly well. Fig. 8 shows the model derived velocity magnitude (color) and direction (vector) showing secondary circulation at cross section in the meander bend near Myrtle Gove. The location of the cross-sections is shown on the right panel of Fig. 8. The vectors shown (left) are tangent to the cross-sections, clearly showing the direction of secondary flow. The white solid line indicates conceptually the expected secondary circulation. The model is in good agreement with the expected secondary circulation.

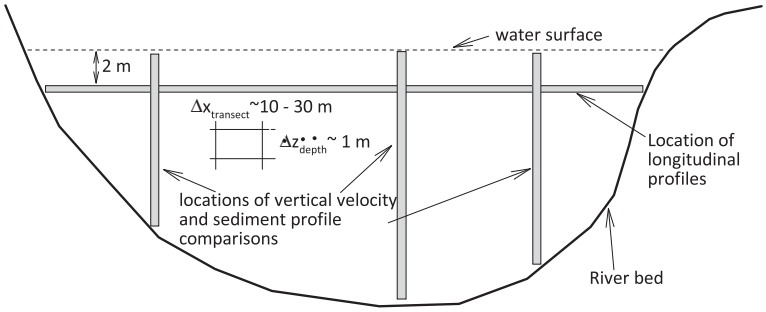

Fig. 6. Schematic showing typical locations along a river transect where velocity and sediment data were compared during calibration and validation with field observations and the model.

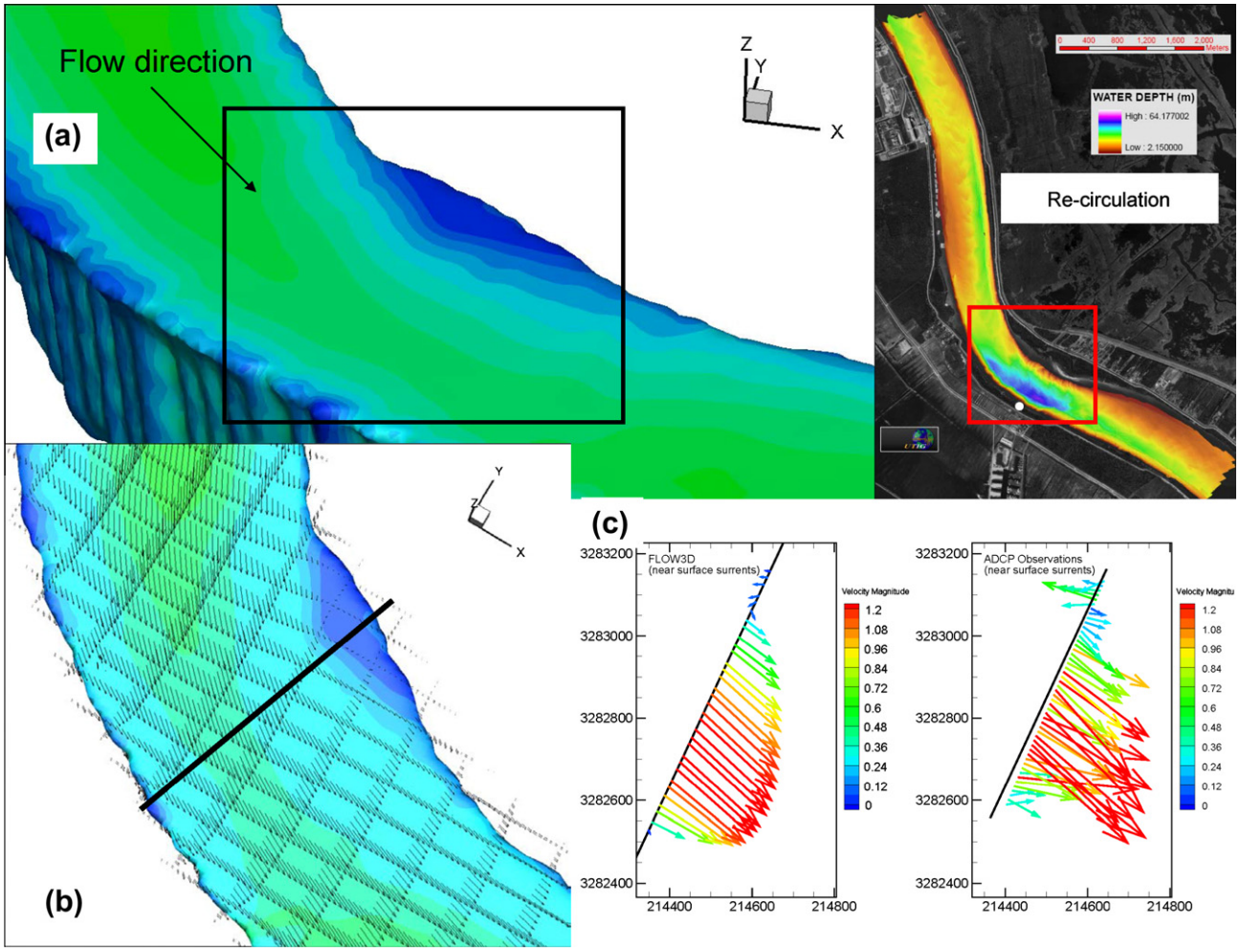

Fig. 7. Model skill assessments on general circulation features. The model, (a) and (b) above, accurately captures the re-circulation zone observed at the meander near Myrtle Grove (c), where the near surface velocity vector (blue sticks) shows the reverse flow pattern (location of transect is shown in (b) with solid white line).

5.3. Model calibration

5.3.1. Velocity calibration

Velocity comparisons were performed at three locations, (1) upstream of the meander in the vicinity of a lateral point bar (*MGup*), (2) near the meander in the vicinity of the deep hole (*MGbend*), and (3) downstream of the meander and the deep hole (*MGdown*). Fig. 9 shows the velocity comparison for the calibration period of April 2009 for discharge of 19,822 cms (700,000 cfs). Fig. 9a shows the location of the ADCP transect, while Fig. 9b and c shows a horizontal velocity profile extracted at 2 m below the water surface, and a vertical velocity profile extracted in the vicinity of the river thalweg at that location, respectively. The model clearly shows good performance, reproducing field velocities within 10–15 cm/s and well within the standard error of the observed fluctuations. A similar performance is shown in Fig. 10, with a vertical and horizontal profile at *MGdown*. The presence of higher variance at this site is evident (Fig. 10), which can be attributed to the high level of turbulence and secondary motion due to the presence deep hole in the outside bend of the channel and bend curvature. Overall, the

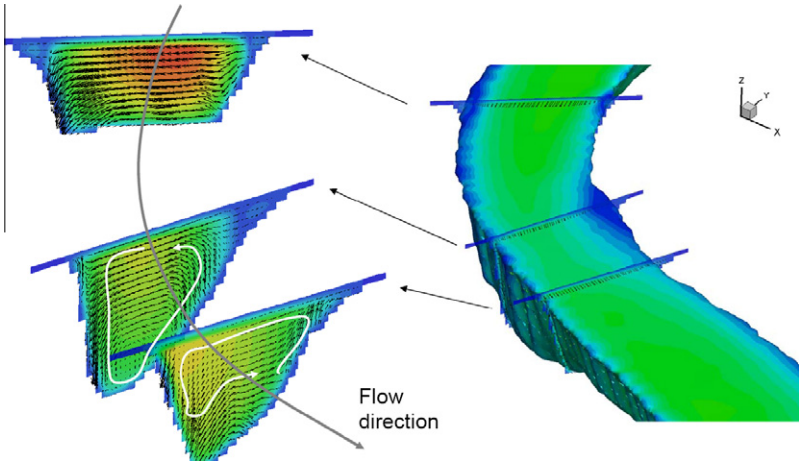

Fig. 8. Model derived velocity magnitude (color) and direction (vector) showing secondary circulation at the meander bend near Myrtle Gove. The location of the cross-sections (left) is shown in the right panel. The vectors shown (left) are tangent to the cross-sections. The black solid vector indicates the dominant downstream flow vector, while the white solid line indicates conceptually the expected secondary circulation.

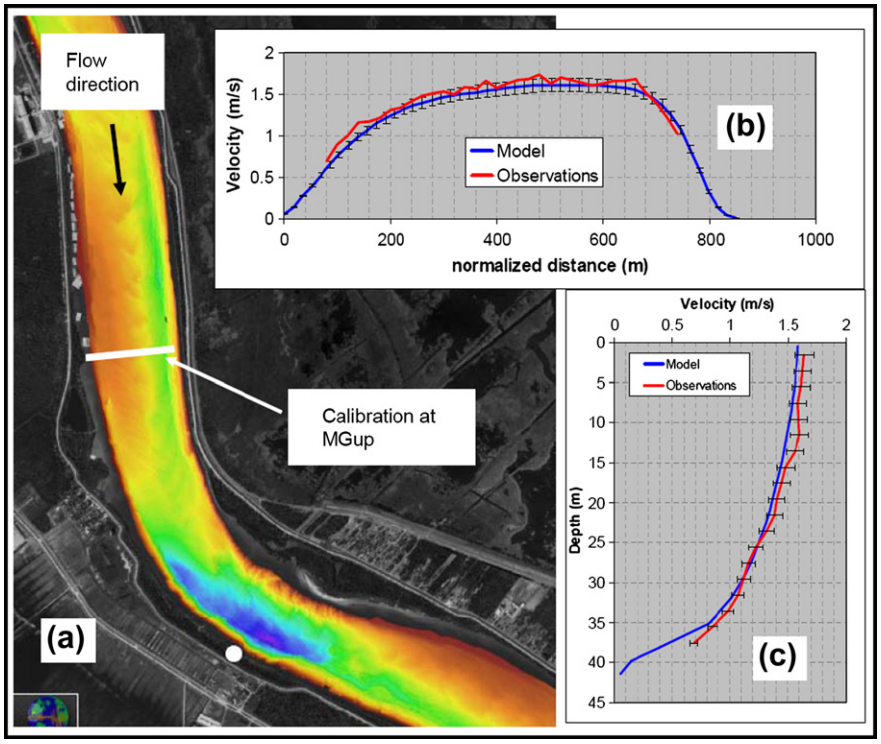

Fig. 9. Calibration for velocity during April 2009 flows at location upstream of the meander (MGup). (a) location of ADCP data; (b) model compared to observations along a horizontal profile extracted at 2 m depth, and (c) model and observations for a velocity profile near the river thalweg.

model results showed good agreement with the field measurements. Root-mean-square error analysis during calibration varied from 0.19 to 0.21 m/s, and $R2$ values resulting from regression lines of observed and modeled velocity between 0.96 and 0.98.

5.3.2. Sediment calibration

The transport of sediment within the study area utilizes discrete particle transport via a non-passive Lagrangian method through an upstream release along the model boundary. At steady state, up to 500,000 particles are tracked within the domain. Particles are weakly coupled to the flow field, which implies that the particles (in their respective classes) are treated as individual particles. The momentum exchange between the flow and the particles focused on the effect of the flow field onto the particles. The concentration of the particles was considered to be small enough not to impact the flow field. Particles released at the upstream end of the model were of various sizes. They were released at a constant rate until a steady state was achieved. The rate of each particle size released at the upstream end was correlated to the measured suspended load of the same size class. As such, the discrete particles were mapped into concentration of each particle size in every computer cell. This processes was repeated with various rates of release to ensure stability of the steady state solution. With total particles of 500,000, 1,000,000, and 1,500,000 tested, it was verified that the sediment spatial distribution for each size class is independent of the particle release rate at the upstream end. The

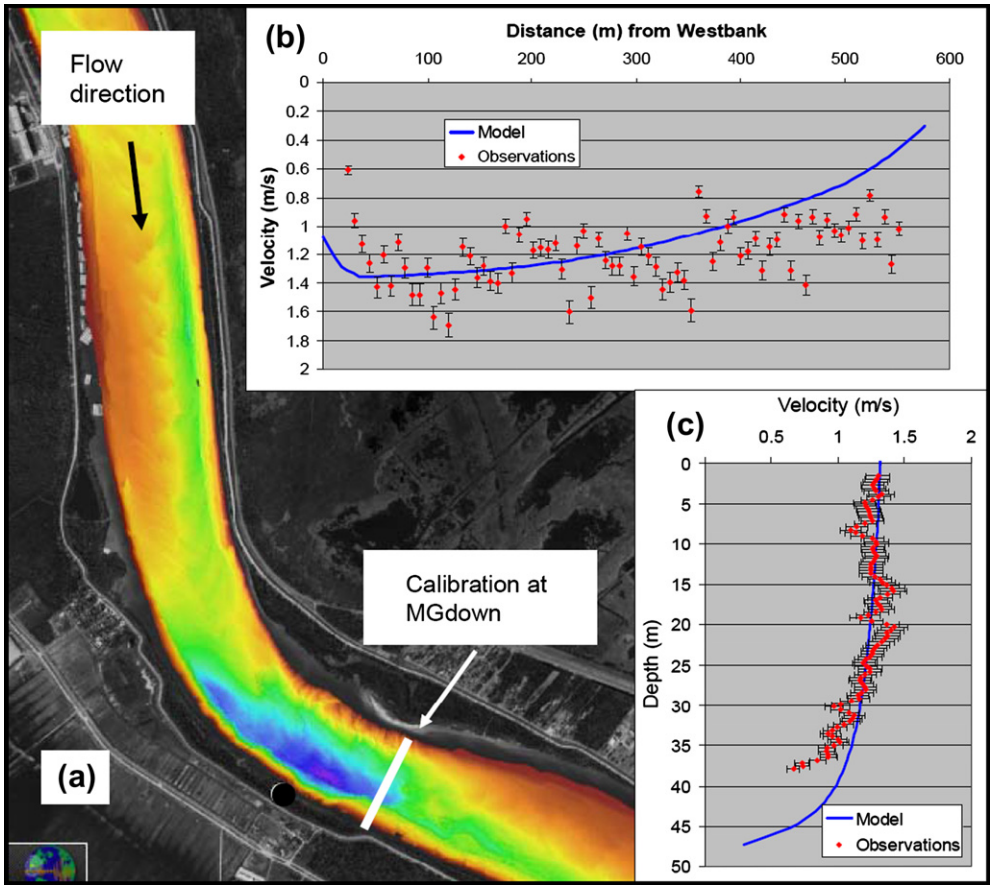

Fig. 10. Calibration for velocity during April 2009 flows at location downstream of the meander (MGdown). (a) location of ADCP data; (b) model compared to observations along a horizontal profile extracted at 2 m depth, and (c) model and observations for a velocity profile near the river thalweg.

process of mapping the discrete particles into concentration is described below.

For a given number of particles in the domain (P_n), among a number of size classes (m) the sediment reference concentration within the domain is a function of the total Volume of Fluid (V_w), the volume of particles (V_p) and the particle density such that:

$$C_{ref}^{m} = P_n V_p \rho_p \tag{8}$$

where C_{ref} is the reference concentration for a number of size classes (m), P_n is the number of particles, V_p is the volume that the particles occupy in the domain and ρ_p is the particle density. To obtain the reference sand concentration, C_{ref}^{s}, Eq. (9) has been used for m classes of sand and silt size particles.

$$C_{ref}^{s} = \sum_{i=1}^{m} (C_{ref}) \tag{9}$$

Hence the normalized concentration is

$$C_s = \frac{C_{ref}}{V_w} = X \tag{10}$$

where C_s is the sand concentration, C_{ref} is the reference concentration, and V_w is the domain water volume. The term, X, is used to derive a conversion factor to transform the model output into concentration directly. The final conversion factor is proportional to the sediment load, which itself is a function of flow intensity. As such, since field measurements are available for the sediment load and total water flow for the calibration and validation events used here, the term X can be easily calculated. The sediment load was calculated based on the detailed isokinetic measurements at MGup. A cross-sectional and depth average of concentration of each size class from the isokinetic samples was estimated in the laboratory for each grain size fraction.

For the sediment load used during calibration, this number is 56.7. It is largely derived by a conversion of the total sediment load to the model domain from tons/d to mg/L. The resulting conversion factor is then used to convert the model derived particle density to a sediment concentration. The FLOW-3D code was modified to complete this computation.

The Lagrangian method used to predict sediment transport utilizes a diffusion coefficient (D), which is often used to predict the dispersive nature of individual particles in natural systems. This coefficient is similar to any other diffusion coefficient in the advection/diffusion equation, and was used in the calibration to produce good model agreement. For the calibration process, the diffusion coefficient was varied from 0.05 to 0.1. To determine the proper diffusion coefficient, three scenarios were run, where $D = 0.05$, 0.075, and 0.1. Once the value which produced satisfactory results was selected, the coefficient remained constant for the validation process. The results from all three simulations are shown in Fig. 11 for upstream of Myrtle Grove at *MGup*, and for downstream of the bend at *MGdown*. The convention for the plot is: left cast is near the right descending bank, and right cast is near the left descending bank. It can be clearly seen in Fig. 11 that the model has a very good ability to reproduce the sand concentration for the April 2009 flow. A small departure is seen between the three simulations with different diffusion coefficients, except for the left cast at *MGdown*. The observations at this site fall within the model simulated concentrations and are therefore considered satisfactory.

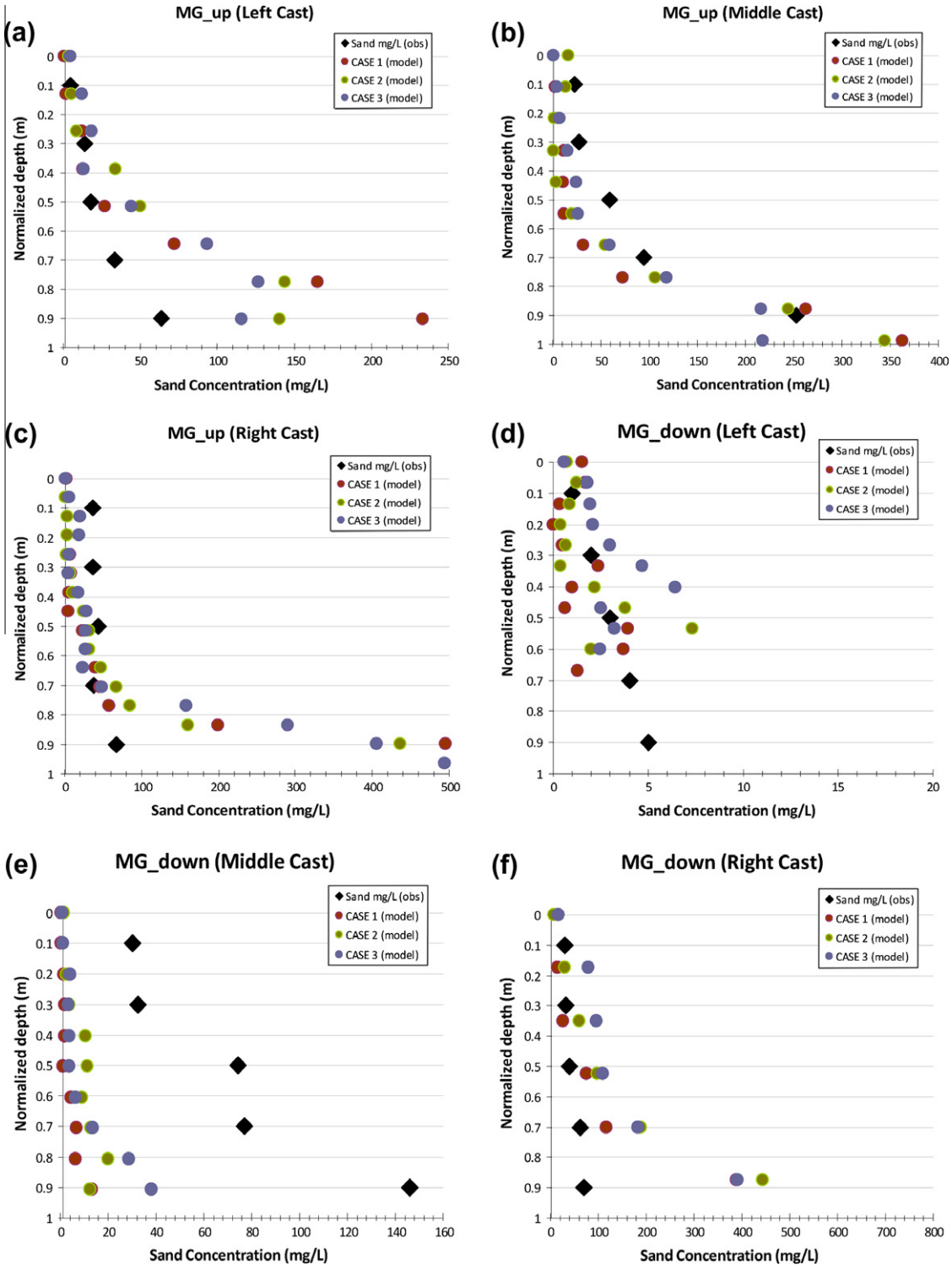

Fig. 11. Suspended Sand comparison between Model (FLOW3D) and observations (Isokinetic P63) at MGup (upstream of the meander) and MGdown (downstream of the meander) for April 2009 flows during model calibration. Diffusion coefficients for lagrangian methods are: Case 1 (D – 0.05), Case 2 (D – 0.1) and for Case 3 (D – 0.075); Convention is: Left cast is near the west-bank, and right cast is near the east-bank.

Overall the predicted sand concentrations compared well with the measurements. However, it was noted that while the surface concentrations of sand are predicted fairly well (except for the middle cast of the *MGdown* transect) the bottom concentrations are often in slight disagreement with the field observations. Therefore, the diffusion coefficient that agreed with observations at the most locations was selected for use in the final simulations. Fig. 11e shows that the model did not accurately capture the observed concentration of sand in the middle of the *MGdown* transect. However, as evident from Fig. 11d and f, the concentrations on either side of that transect are reproduced well. Furthermore, the small disagreement between the model and observations near

the bed at Fig. 11a appears not to be a concern since after the transition through the meander, the concentrations are reproduced. This response is likely due to the combined effect of (a) much higher uncertainties in observations due to the influence of turbulent fluctuations of the bed material load compared to other depths, and (b) due to higher re-suspension of bed material at this site.

5.4. Validation

The spring flood of 2010 was selected to perform a validation of the model for velocity distribution and sediment transport. The field measurements started on April 13th and ended on the 16th. Not all locations where measurements were taken in the April 2009 were repeated during the April 2010 field surveys. Hence comparisons with observations are shown here for *MGup* location only. During the validation, no adjustment of any parameter was performed.

5.4.1. Velocity validation

Velocities (both vertical and horizontal profiles) were extracted at the locations where field data were available and compared to model simulated velocities. Fig. 12 shows the velocity comparisons between observations in April 2010 during stationary ADCP surveys. The surveys have approximately 15–30 min long sampling periods and approximately 800–1700 data-points of velocity for each 0.5 m depth (0.5 m of depth equals one bin). The panels (a) through (c) in Fig. 12 show these velocities as points, while the error bars show the standard deviation for each bin for the entire sampling period. It is evident that the velocity profiles are fairly stable, and generally exhibit different variance. For instance, at the shallower *MGup1* location, towards the right descending bank over the point bar, there is more variance (as indicated by the error bars) near the surface of the water compared to the thalweg at site *Mgup3* where ADCP data show higher variance near the bed. Generally however, there is a standard deviation of at least 0.2–0.4 m/s.

The model's performance during validation appears to be satisfactory and generally within or near the edge of the uncertainty or dispersion observed in the field. For instance, as can be seen in Fig. 12a, the model slightly under predicts the velocity near the bed, and agrees well with the measurements at depths of approximately 12–16 m, but over estimates the surface velocity by 0.2 m/s. A slightly different behavior is seen at the center point (MGup2 – Fig. 12b) where the surface velocity are in very good agreement with observations, while near the bottom the model slightly under-predicts the velocity field. The deviation near the bed indicates the possibility that the bed form roughness for this section and flow event was not consistent with the calibration case. In the thalweg of the river (MGup3, Fig. 12c), the model is in very good agreement with observations with a small under-prediction of approximately 0.05 m/s. This is verified further by comparison of the horizontal velocity profile shown in Fig. 12d. It can be clearly seen here that the edge velocities near the banks compare very well with observations, while the velocity field near the deeper part of the river is generally in agreement except for a small under-prediction in the deepest part of the channel. This is consistent with the velocity profile shown in Fig. 12a and b. Overall however, both vertical and horizontal velocity profiles agree well with

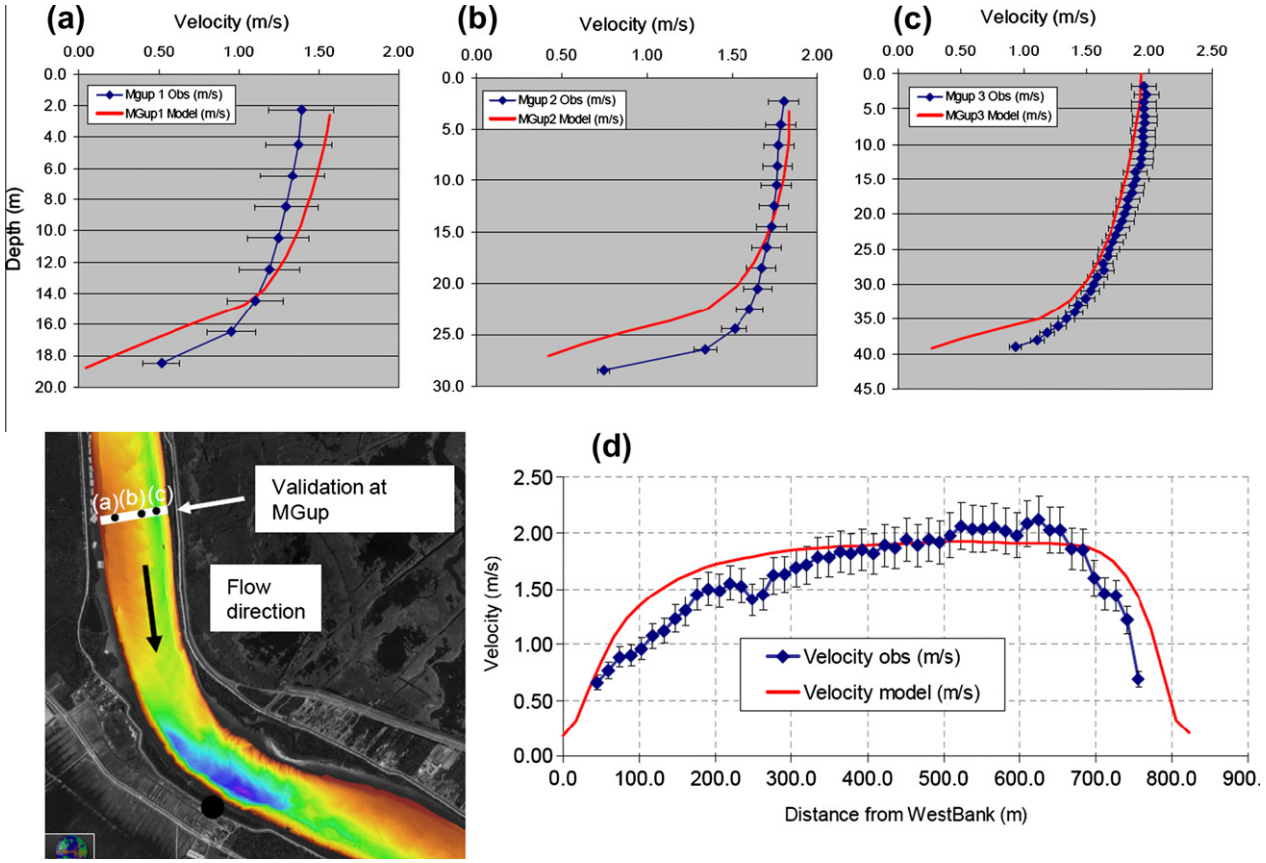

Fig. 12. Velocity validation during the spring April 2010 flows. Panels (a) through (c) are from time-averaged stationary ADCP surveys at MGup location 1, 2 and 3 (from Allison, 2011) and shown in solid circles in regional view. Panel (d) shows the horizontal velocity comparison between the model and observations at 2 m below the water surface. Data for this comparison were from ADCP transect surveys (from Allison, 2011).

observations with root-mean-square error from 0.14 to 0.25 m/s, and $R2$ values resulting from regression lines of observed and modeled velocity between 0.73 and 0.94.

5.4.2. Sediment validation

A similar methodology to that previously described during calibration was utilized to process, analyze and extract sediment concentrations for use in comparisons with the field measurements. Fig. 13 shows the suspended sediment concentration predicted by the model during the validation period (red triangles), compared to field observations (blue diamonds) collected at the upstream cross-section at (*MGup* sites). The model's ability to reproduce observed concentrations appears satisfactory, with good agreement throughout the water column at all three sites. There is a small over-prediction of sand concentrations near the bed at *MGup1* (over the point bar), as can be seen in Fig. 13a, but the model does well in predicting sand concentrations for 90% of the water column. At the center of the river (site *MGup2* – Fig. 13b) the model is predicting sand concentrations well near the surface and near the bed, but slightly under-predicts at around 30% depth. This however, is potentially due to a higher uncertainty in the field observations as shown by a sudden increase in sand concentration at the 30% depth. At *MGup3* (Fig. 13c) a similar performance by the model and a similar increase in the observed suspended sand concentrations is seen around 30% of the water column. Besides this disagreement at this depth, the model performance in predicting sediment concentrations throughout the water column is reasonable. It is important to mention that there are no duplicates of isokinetic sampling or multiple samples at any locations, and therefore it is difficult to assess the field uncertainty. However, from Allison (2011) the expected uncertainty is proportional to the river turbulence, flow depth, and other parameters. Repeated field campaigns show that the variations can be of the order of 10% of the measured concentrations near the surface, and as much as 50% of the measured concentration near the bed and at high discharges.

6. Diversion scenarios

Once calibrated and validated, the model was used to test various diversion designs. The numerical experimentations included various alignments, intake locations, and sizes of the intake channel and diversion structure.

Three diversion sizes were tested here. The maximum (design) capacities of these diversions are: 424.75, 1274.26, and 2123.76 cms when the river discharge is at 28,317 cms or higher. The river flow conditions were tested for a flow discharge of 19,822 cms and as such, the diversion structures were assumed to be operating below the design capacity.

6.1. First alignment (RK96.9) [OA-RK96.9-15K]

The general layout of the design is shown in Fig. 2. To facilitate the discussions of the various modeling scenarios, each scenario will be designated by a title that reflects its intake location and design capacity. As such, the full description of this scenario is Original Alignment with an intake at RK96.9 and with a design capacity of 424.75 cms (15,000 cfs). Hence it will be designated as OA-RK96.9-15K. The diversion channel was designed such that it would carry a flow of 424.75 cms. It should be noted that the design did not include (explicitly) the energy losses due to bends along the length of the diversion channel and due to the transitions from one cross section shape/size to another.

The April 2009 event (same event that was used to calibrate the model) was used to assess the performance of this design. A tail-water elevation of 1.524 m-NAVD88 was set at the downstream end of the diversion channel (bay side). This estimate reflects typical conditions observed in the bay side. The entrance of the intake channel at the river side is set at an elevation of −12.2 m-NAVD88. The channel gradually slopes up to an elevation of −7.62 m-NAVD88 at the bay side. Immediately after the entrance from the riverside, the channel has rectangular cross section with a width of 9.14 m. The channel then transitions into a trapezoidal cross section (bottom width = 9.14 m, and side slope of 3:1 (H:V). The channel has two bends as shown in Fig. 2. The channel cross section transitions into a trapezoidal cross section with bottom width = 9.14 m, and a compounded side slope of 3.7:1 and 4.7:1 (H:V).

A nested grid (multi-grid) approach was used to capture the flow field within the narrow intake of the diversion channel. Fig. 14 shows the details of the flow field as captured by the numerical model. The energy losses captured by FLOW-3D due to the bends and cross section transitions showed that the diversion channel capacity was lower than nominal design. For the river conditions used in this case (River flow = 19,821 cms), River tail-water = 1.9 m-NAVD88, diversion channel tail water = 1.524 m-NAVD88), the flow captured by the diversion channel was 322 cms.

Following a sediment simulation, and to test the ability of the diversion channel to capture various sediment size classes, the sediment load for every size class that was captured in the diversion channel has been calculated using the model. The sediment load reported here is at the terminal end of the diversion channel at the bay side, hence it represents the amount of sediment that reaches the bay. A summary of the sediment load captured in the diversion channel is shown in Table 1.

The main objective of this diversion project is to build land, thus the primary goal is to maximize the sediment load captured by the diversion channel. It is also critical to maximize the ratio of sediment load to water extracted by the diversion channel to minimize

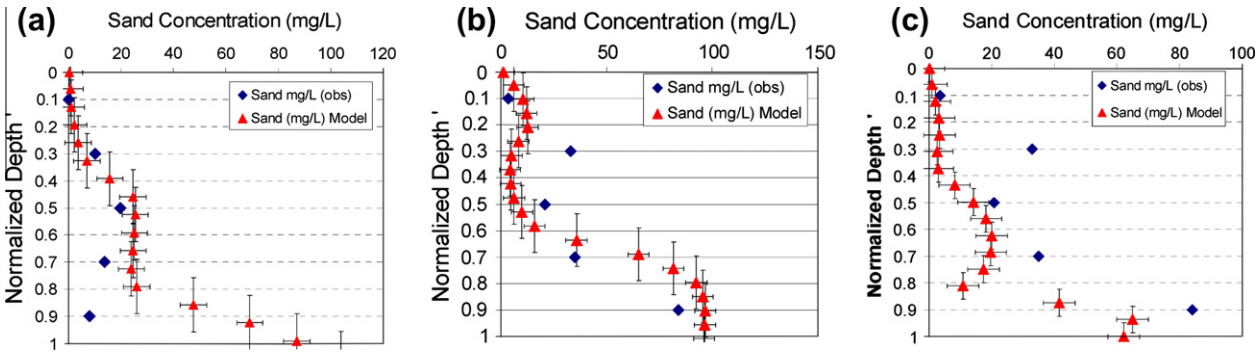

Fig. 13. Suspended sediment (sand only) validation during the April 2010 flows. The field data were collected using P-6 sampler on April 14, 2010 (Allison, 2011). The locations are respectively (a) MGup1, (b) MGup2, and (c) MGup3.

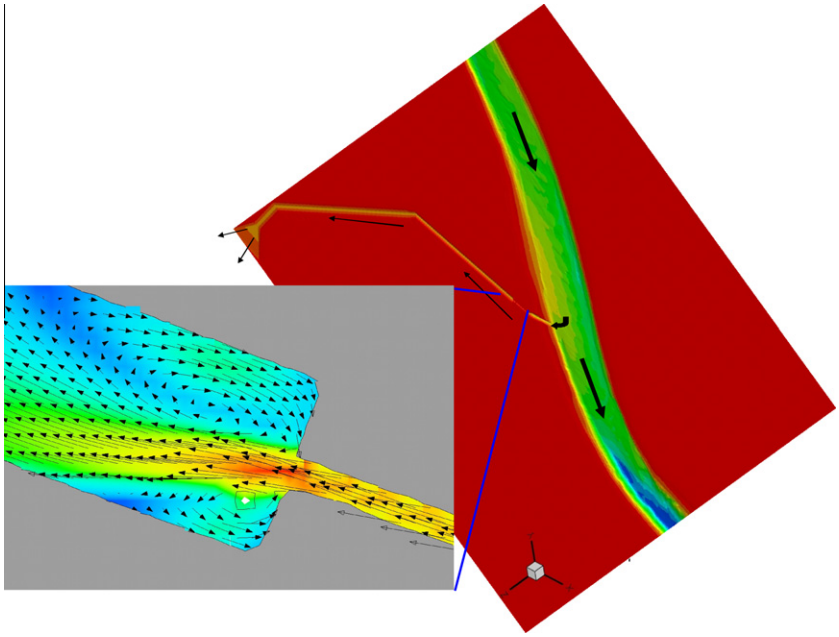

Fig. 14. Details of the flow field at transition zone from the rectangular segment of the diversion channel into the trapezoidal segment [OA-RK96.9-15K].

(or completely eliminate) the potential of shoaling downstream of the diversion intake. The following indicator was used to assess the performance of each diversion design tested in this study:

$$SWR = \frac{Sand\,Load\,Diverted/Sand\,load\,in\,the\,River}{Water\,Discharge\,Diverted/Water\,Discharge\,in\,the\,River} \quad (11)$$

where SWR is the sand/water ratio. As indicated above, the goal is to maximize SWR since the higher the value of SWR the lower the potential of shoaling in the river. As shown in Table 1, this design extracted 1.62% of the main river water discharge, while it only extracted 1.19% of the main river silt load, and 0.42% of the main river sand (size range 63–250 μm) load. As such, SWR is 0.26. This is not a favorable ratio and is indicative of a poor efficiency of this design to extract an adequate amount of sediment from the River.

6.2. Modified alignment (RK97.7)

A modified alignment was proposed to increase the diversion's ability to capture sediment and improve the sediment–water ratio in the diversion channel as compared to the sediment–water ratio in the main stem of the river. The intake of the diversion channel was moved upstream approximately 800 m. This adjustment placed the intake at the downstream end of the sand bar on the right-descending bank (Alliance South). Furthermore, bends were removed from the alignment (see Fig. 2), reducing the energy losses along the length of the diversion channel.

Several designs were tested for this alignment. The first test was for a diversion channel with a capacity of 1274 cms. This design was tested with and without the earthen guide dike to assess its ability to enhance the performance of the diversion. Other tests include a diversion channel with a capacity of 424.75 and 2123.76 cms.

The first test performed for this alignment was the 1274 cms case with the guide dike in place The bottom width of the trapezoidal channel was 27.4 m and the side slopes were 3:1 (H:V). The channel transitioned to a trapezoidal channel with a bottom width of 27.4 m and a compounded side slope.

The same river conditions that were used for the Original Alignment were used here for the modified alignment (River flow = 19,821 cms, River tail-water = 1.9 m-NAVD88, diversion channel tail water = 1.524 m-NAVD88. As mentioned before, for a nominal discharge of 28,317 cms in the river, the design capacity of the diversion channel is 1274 cms (45,000 cfs), however, under the flow conditions used in this test (River flow of 19,821 cms), the flow captured by the diversion channel was 955 cms. A summary of the sediment load captured in the diversion channel is shown in Table 1.

As shown in Table 1, this design extracted 4.82% of the main river water discharge and 6.55% of silt, and 4.14% of sand (size range 63–250 μm). This performance is more favorable (SWR = 0.85) compared to the Original Alignment.

For the simulation of the 1274 cms modified alignment design, it was observed that the earthen dike at the intake of the diversion created a large eddy in the main stem of the river and a sediment buildup on the downstream side of the diversion. To avoid this problem, the dike was removed, and a simulation was performed without the dike in place. This simulation was labeled "ND" for "No Dike" (ND-RK97.7-45K). Table 1 provides a summary of the sediment load captured in the diversion channel without the dike. Removing the dike slightly lowered the water discharge to 4.73% of the total river discharge. The dike created a stagnation point and built up the water stage at its upstream face, creating a favorable head-differential and improving the total water discharge in the diversion channel. However, this advantage is not significant as can be seen in the with- and without-dike simulations, 4.82% and 4.73% respectively.

The ND-RK97.7-45K alignment extracted slightly lower silt load; 5.92% of the main river silt load compared to 6.55% obtained with the MA-RK97.7-45K. However, the ND-RK97.7-45K alignment improved the sand load (range of 63–250) extracted in the diversion channel compared to the MA-RK97.7-45K alignment, namely 4.39% and 4.14% respectively. Overall, for this design the SWR is 0.93.

The dike does not appear to be a critical component of the design. In fact, it is detrimental for the transport of some size classes. Hence, it is recommended to remove the dike, given the negative

Table 1
Summary of the sediment load (for every size class) captured by the three alternative diversion channel alignments.

	Mississippi River (main stem)	Diversion channel OARM60.2-15K	Diversion channel NDRM60.7-15K	Diversion channel MARM60.7-45K	Diversion channel NDRM60.7-45K	Diversion channel NDRM60.7-75K
Water discharge (m^3/s)	19,821	322	361	955	937	1725
Water discharge (CFS)	700,000	11,369	12,733	33,735	33,075	60,918
Sediment load (metric tons/d) – 32 μm	233,539	2786	4189	15,306	13,819	24,789
Sediment load (metric tons/d) – 63 μm	10,839	104	188	663	619	1156
Sediment load (metric tons/d) – 96 μm	21,816	144	335	1230	1150	2357
Sediment load (metric tons/d) – 125 μm	34,437	133	420	1637	1675	3726
Sediment load (metric tons/d) – 250 μm	23,460	2	44	218	528	1607
Total 63–250 μm load (metric tons/d)	90,554	383	987	3748	3972	8847
Sediment/water ration (SWR)		0.26	0.60	0.85	0.93	1.12

impacts it has on the flow field in the river and the lower efficiency to extract larger sediment grain sizes.

6.3. Additional diversion scenarios

In this section, the results of two additional simulations are presented, namely, ND-RK97.7-15K, and ND-RK97.7-75K. The two simulations were performed using the same flow conditions of all the other diversion scenarios. As such, direct comparisons can be made among all the diversion scenarios. Table 1 shows the results of these two simulations.

The results presented in Table 1 clearly show that the performance of the modified alignment is better than the original alignment. The ND-RK97.7-15K diversion delivered approximately 150% silt load compared to the OA-RK96.9-15K diversion. The level of improvement increased for the larger sediment size classes making this design more favorable for larger size classes. The SWR for the 424.75 cms diversion improved from 0.26 for the original alignment to 0.60 for the modified alignment. However, it should be noted that even with the modified alignment, the SWR is low. To minimize shoaling and other undesirable impacts, a SWR value of at least 1 is necessary. The results presented in Table 1 indicate that the larger the amount of water diverted, the higher the value of SWR. Table 1 shows that the 2123.76 cms (75,000 cfs) diversion extracted 9.77% of the sand load from the river while only extracting 8.7% of the river water, i.e. SWR of 1.12. This higher ratio (larger than 1) is encouraging as it implies little potential problems with shoaling in the river as a result of the diversion.

As can be seen in Table 1, the Original Alignment did not perform well in terms of capturing equal amount of sediment load compared to the water flow. The performance of this alignment was impacted by the location of the intake and the orientation of the alignment (adverse angle to the flow direction in the river). The intake is located on the outside of the Myrtle Grove bend (right descending bank), where the sand material has already started to migrate from the right to the left descending bank. This alignment design also contained two bends that induced energy losses which resulted in a reduction of the water and sediment carrying capacity of the diversion channel.

The modified alignment promoted the extraction of sand material from the vicinity of the point sand bar before it starts to migrate towards the left descending bank. Further, the modified alignment had a favorable angle relative to the flow direction in the river. Hence, it produced a more favorable water-to-sediment ratio. The modified alignment (Table 1) improved the SWR from 0.26 to 0.60 for the original alignment, leading to the conclusion that SWR is proportional to water flow, ie, the larger the diversion size, the higher the SWR. Comparing design flows of the order of 424.75, 1274.26, and 2123.76 cms, respectively, for the modified alignment (all without the guide dike), the SWR improved from 0.60 to 0.93 to 1.12.

It was observed that the dike component of the modified alignment design had an adverse effect on the flow field in the river (large eddy and potential sediment buildup on the downstream side). Thus, the dike was removed and the performance of the diversion was tested without it (run ND-RK97.7-45K). The results indicate that the dike does not enhance the performance of the diversion significantly. In fact, for some of the larger sediment size classes, the presence of the dike prevented sediment from entering the diversion channel. Removing the dike, however, improved the SWR from 0.85 to 0.93. Therefore, this study confirmed that removal of the dike from the design will be beneficial to the project from as it regards to sediment extraction, but also with regard to reducing overall cost.

7. Conclusions

The analyses in this paper provides an insight into the water flow and sediment dynamics near diversions and shows how this insight can be used as a guide to the setting and design of a land-building diversion. The paper includes the setup, calibration, validation, and application of a three-dimensional numerical model to perform the analyses. Detailed field measurements of velocity and sediment concentrations were critical in setting up and calibrating the numerical model.

The FLOW-3D model was selected for this study because it adequately represents physical processes. A major reason for selecting Flow3D is that it permits the accurate incorporation of control structures in the transcritical free surface flows associated with large scale diversions. Further, the accuracy of the VOF approach in Flow3D is important in such applications. The model results compared well with the field observations, resolved complex flow features observed in the field, such as the strong eddy at the Myrtle Grove bend, and predicted the complex vertical distribution of sediment concentration profiles. The model was used to assess the performance of various diversion sites, alignments and sizes.

The study demonstrated that the sand sediment–water ratio for a diversion at the outside of the meander bend was 0.26 while for a diversion at the reach upstream of the meander the SWR is in the range of 0.85–1.15 depending on the diversion orientation and capacity. A SWR greater than 1 is required to minimizes the shoaling impact. Further, placing the diversion on top of a sandbar resulted in a significant increase in the sediment–water ratio. Additional intake designs should be considered to improve the SWR. Since the upper layers of the water column carry the least amount of sand (and therefore have a small contribution to the sediment load), it is recommended that an orifice-like entrance be investigated. Such a design will draw water from the deeper and more sand rich layers and can be a good alternative to designs investigated herein. Significant improvement to the SWR will be cost effective if it avoids shoaling downstream of the structures, and contributes to lower dredging costs in the River, and poses small concerns with regard to navigation.

It should be noted that the analyses performed herein focused on the potential local (near-field) impact of the diversion and in optimizing the design of the intake structure in terms of size and location. The large-scale (far-field) and long-term (decadal) impacts are not addressed in this study, but are currently being addressed through a parallel modeling effort using low-resolution regional three-dimensional and one-dimensional analyses. The results of that parallel effort will be presented in future publications.

References

ABFS, 1982. Atchafalaya Basin Floodway System, Louisiana. Feasibility Study. U.S. Army Corps of Engineers, New Orleans District, 4 volumes.

Allison. M., 2011. Interpretative Report on Water and Sediment Surveys of the Mississippi River Channel Conducted at Myrtle Grove and Magnolia in Support of Numerical Modeling, October 2008–May 2010. State of Louisiana Office of Coastal Protection and Restoration.

Allison, M.A., Meselhe, E.A., 2010. The use of large water and sediment diversions in the lower Mississippi River (Louisiana) for coastal restoration. J. Hydrol. 387, 346–360.

Barras, J., Beville, S., Britsch, D., Hartley, S., Hawes, S., Johnston, J., Kemp, P., Kinler, Q., Martucci, A., Porthouse, J., Reed, D., Roy, K., Sapkota., S., Suhayda, J., 2003. Historical and Projected Coastal Louisiana land Changes: 1978–2050. U.S. Geological Survey Open File Report 03–334, 39 p (revised January 2004).

Barras, J.A., 2009. Land Area Change and Overview of Major Hurricane Impacts in Coastal Louisiana, 2004–08: U.S. Geological Survey Scientific Investigations Map 3080, scale 1:250,000, 6 p. pamphlet.

Barkhudarov, M.R. 2004. Lagrangian VOF Advection Method for FLOW-3D®. Flow Science Technical Note #63, Flow Science, Inc. <http://www.flow3d.com/pdfs/tn/FloSci-TN63R>.

Coleman, J., Roberts, H., Stone, G., 1998. The Mississippi River delta; an overview. J. Coast. Res. 14 (3), 698–716.

Davis, M. 2010. Numerical Simulation of Unsteady Hydrodynamics in the Lower Mississippi River. University of New Orleans Thesis. May 2010.

Day, J.W., Shaffer, G.P., Britsch, L.D., Reed, D.J., Hawes, S.R., Cahoon, D., 2000. Pattern and process of land loss in the Mississippi Delta: a spatial and temporal analysis of wetland habitat change. Estuaries 23 (4), 425–438.

Flow Science, 2010. FLOW-3D – Excellence in Flow Modeling Software. User Manual 9.4 Volumes 1 and 2. Santa Fe, NM 87505. <www.flow3d.com>.

Gagliano, S., Meyer-Arendt, K., Wicker, K., 1981. Land loss in the Mississippi River delta plain. Trans.-Gulf Coast Assoc. Geol. Sci. 31, 295–300.

Hirt, C.W., Nichols, B.D., 1981. Volume of fluid (VOF) method for the dynamics of free boundaries. J. Comput. Phys. 39, 201.

Hirt, C.W., Sicilian, J.M., 1985. A porosity technique for the definition of obstacles in rectangular cell meshes. In: Proc. Fourth International Conf. Ship Hydro., National Academy of Science, Washington, DC, September.

Hirt, C.W. 1999. Particle-Fluid Coupling. Flow Science Technical Note: FSI-99-TN50. <http://www.flow3d.com/pdfs/tn/FloSci-TN50.pdf>.

Kheiashy, K., McCorquodale, J., Georgiou, I., Meselhe, E., 2010. Three dimensional hydrodynamic modeling over bed forms in open channels. Int. J. Sedim. Res. 25 (2010), 431–440.

LACPR, 2009. Final Technical Report of the Louisiana Coastal Protection and Restoration Study, U.S. Army Corps of Engineers, New Orleans District. <http://lacpr.usace.army.mil/>.

Lane, R.R., Day, J.W., Day, J.N., 2006. Wetland surface elevation, vertical accretion, and subsidence at three Louisiana estuaries receiving diverted Mississippi River water. Wetlands 26, 1130–1142.

LCA, 2004. Louisiana Coastal Area (LCA), Louisiana: Ecosystem Restoration Study; 1: LCA Study—Main Report. New Orleans, LA: New Orleans District.

Meselhe, E.A., Habib, E.H., Griborio, A.G., Chen, C., Gautam, S., McCorquodale, J.A., Georgiou, I.Y., Stronach, J.A., 2005. Multidimensional Modeling of the Lower Mississippi River. Estuarine and Coastal Modeling.

Meselhe, E.A., Sotiropoulos, F., 2000. Three dimensional numerical model for open channels with free surface variations. J. Hydraul. Res. IAHR 38 (2).

Meselhe, E.A., Weber, L.A., Odgaard, A.J., Johnson, T., 2000. Numerical modeling for fish diversion studies. J. Hydraul. Eng. ASCE 126 (5).

MRSNFR, 2000. Mississippi River Sediment, Nutrient, and Freshwater Redistribution Feasibility Study. U.S. Army Corps of Engineers, New Orleans District.

Muste, M., Meselhe, E.A., Weber, L., Bradley, A.A., 2001. Coupled physical-numerical analysis of flows in natural waterways. J. Hydraul. Res. IAHR 39 (1).

Pereira, J.F., McCorquodale, J.A., Meselhe, E.A., Georgiou, I.Y., Allison, M.A., 2009. Numerical simulation of bed material transport in the Lower Mississippi River. J. Coast. Res. (56), 1449–1453.

Rego, J., Meselhe, E.A., Stronach, J., Habib, E., 2010. Numerical modeling of the Mississippi-Atchafalaya Rivers' sediment transport and fate: considerations for diversion scenarios. J. Coast. Res. 26.

U.S. Army Corps of Engineers, 1984. Mississippi and Louisiana Estuarine areas: Freshwater Diversion to Lake Pontchartrain Basin and Mississippi Sound-Feasibility Study. New Orleans District.

Yakhot, V., Orszag, S.A., 1986. Renormalization group analysis of turbulence. I. Basic theory. J. Sci. Comput. 1, 1–51.

Yakhot, V., Smith, L.M., 1992. "The Renormalization Group, the e-Expansion and Derivation of Turbulence Models". J. Scientific Computing 7, 35–61.